Entanglement in Resonance Fluorescence

Check for updates

Juan Camilo López Carreño[1] ✉, Santiago Bermúdez Feijoo[2] & Magdalena Stobińska[3]

Particle entanglement is a fundamental resource upon which are based many quantum technologies. In this Article, we introduce a new source of entangled photons based on Resonance Fluorescence delivering photon pairs as a superposition of vacuum and the Bell state $|\Phi^-\rangle$. Our proposal relies on the emission from the satellite peaks of a two-level system driven by a strong off-resonant laser, whose intensity controls the frequencies of the entangled photons. Notably, such a frequency tuning can be done without decreasing the degree of entanglement between the photons and, unlike current technologies, the intensity of our source can be increased without the risk of spoiling the signal by including higher-order processes into the emission. Finally, we illustrate the power of our novel source by exciting an ubiquitous condensed-matter system, namely exciton-polaritons, and show that they are left in a maximally entangled steady state.

Resonance Fluorescence, the interaction between a two-level atom and coherent light, has been the subject of fundamental research from the early stages of quantum optics[1,2]. In particular, the observation of photon antibunching from this interaction[3] paved the way for investigations regarding the quantum character of light, as well as the phenomena that has enabled, for instance, the pursue of optical transistors based on single photons[4]. In turn, the latter are a key element for many quantum information technologies[5,6], allowing the possibility to design protocols for, e.g., quantum teleportation[7] and quantum cryptography[8]. Typically, Resonance Flourescence is implemented when a laser (with a well defined energy) effectively matches a single atomic transition. Therefore, in practice, one deals with the excitation of a so-called "two-level system" (2LS). Thus, the laser can only induce a single excitation in the atom at the time, which has led Resonance Fluorescence to be regarded as an ultrabright source of quantum light[5,9,10], with high single-photon purity[11,12]. However, recent investigations that analysed the luminescence with spectral resolution[13], have found that the emission form a 2LS actually consists of multiple highly-correlated photons[14–20]. Such a multi-photon structure is particularly revealed when the intensity of the driving laser is strong and the 2LS enters into the so-called *Mollow regime*[21], in which the emission spectrum of the 2LS consists of a triplet, as illustrated in dashed lines in Fig. 1a. Experimentally, such a spectrum has been observed in a variety of platforms, including quantum dots[22–27], molecules[28], cold atom ensembles[29], confined single atoms[30], photonic chips[31], and superconducting qubits[32–34] (and 2LSs can also be constructed in other platforms including superconducting circuits[35–41] and photonic structures[42–44]), thus covering a wide range of energies of operation.

In this article, we demonstrate that time-frequency entanglement can be extracted from Resonance Fluorescence, specifically, from the bare emission of a Mollow triplet, without the need to recurring to atomic collections[45], nor altering the internal structure of the 2LS by considering its biexciton structure[46] or coupling it to a cavity[9,47–51]. Our analysis is based on the recent finding that, although the photons emitted from a 2LS are perfectly antibunched, observing finite frequency regions of the emission allows to unveil a rich underlying landscape of photon correlations[14–16]—ranging from antibunching to superbunching statistics, passing through thermal and uncorrelated light. In fact, the statistical variability of the photons emitted by resonance fluorescence allows to design exotic sources of light[52], excite other optical targets[53–55], and perform the so-called *Mollow spectroscopy*[53], whereby, e.g., the internal structure of complex and highly-dissipative quantum systems can be probed with a minimal amount of photons, namely, two. Here, instead, we show that when the 2LS is driven out of resonance, the emission from the sidebands of the triplet behave as a heralded source of entangled photon pairs, as sketched in Fig. 1b. Thus, we find that our source can operate at high intensities without spoiling the entanglement with higher-order processes, and that the emitted photon pairs follow an antibunched statistics (instead of an uncorrelated one, as in SPDC sources). Finally, given variety of platforms on which the Mollow triplet has been implemented, our source is able to operate on a wide gamut of frequencies (cf. Table 1 in the Methods section for details) and to interface with, e.g., condensed-matter systems that can benefit from entangled excitation[56], thus making resonance fluorescence a compelling alternative to the existing sources of entangled photons.

[1]Institute of Theoretical Physics, University of Warsaw, ul. Pasteura 5, 02-093 Warsaw, Poland. [2]Departamento de Física, Universidad Nacional de Colombia, Ciudad Universitaria, K. 45 No. 26–85 Bogotá D.C., Colombia. [3]Faculty of Mathematics, Informatics and Mechanics, University of Warsaw, ul. Banacha 2, 02-097 Warsaw, Poland. ✉e-mail: juclopezca@gmail.com
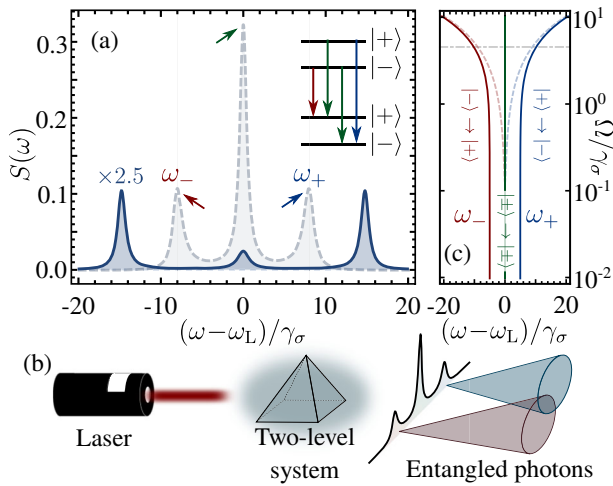
Fig. 1 | The Mollow triplet driven out of resonance. a Emission spectrum when the laser is resonant (dashed) and detuned (solid) from the 2LS. The emission lines are identified with the four possible transitions (two of them are degenerate) between the dressed states (shown in the inset). **b** Scheme of our proposed source of entangled photon pairs emitted from the sidebands of the Mollow triplet. **c** Energy transitions enabling the emission from the 2LS as a function of the driving intensity. In the detuned case (solid, dark lines), and as opposed to the resonant one (dashed, light lines), the satellite peaks become the dominant feature of the spectrum, and the dynamics is given by transitions that change the quantum state of the 2LS, i.e., by transitions of the type $|\pm\rangle \to |\mp\rangle$ (shown in red and blue). For the figure we used γ_σ as the unit, $\Omega/\gamma_\sigma = 4$ (marked in (**c**) as an horizontal dash-dotted gray line) and $(\omega_\sigma - \omega_L)/\gamma_\sigma = 25/2$.

The rest of this Article is organized as follows: We first describe the dynamics of our source and then we demonstrate that energy-time entanglement between photons emitted from the sidebands of the 2LS is unveiled simply by including the observation of the light into the description of our system. Next, we use a quantum Monte Carlo simulation to demonstrate that, as a consequence of the detuned excitation, the entangled photon pairs are heralded. Finally, we show that our source is able to drive complex condensed-matter systems (e.g., exciton-polaritons[57]) into a maximally entangled steady state, despite them being immersed within a highly-dissipative environment.

Results

Description of the source

Our source of entangled photons is based on the excitation of a 2LS with natural frequency ω_σ driven off-resonantly by a laser with intensity Ω and frequency $\omega_L = \omega_\sigma - \Delta$, namely, the detuning between the 2LS and the laser is $\Delta = (\omega_\sigma - \omega_L)$. Formally, the dynamics of our source is described by the Hamiltonian (we take $\hbar = 1$ along the paper)

$$H_\sigma = \Delta\sigma^\dagger\sigma + \Omega(\sigma^\dagger + \sigma), \qquad (1)$$

where $\sigma^\dagger$ and σ are the creation and annihilation operators of the 2LS, which follow the pseudo-spin algebra. The dissipation of the system is taken into account through the master equation

$$\partial_t\rho = i[\rho, H_\sigma] + \frac{\gamma_\sigma}{2}\mathcal{L}_\sigma(\rho). \qquad (2)$$

Here, H_σ is the Hamiltonian in Eq. (1), γ_σ is the decay rate of the 2LS and $\mathcal{L}_\sigma(\rho) \equiv 2\sigma\rho\sigma^\dagger - \rho\sigma^\dagger\sigma - \sigma^\dagger\sigma\rho$. When the intensity of the driving is sufficiently large (that is, when $\Omega > \gamma_\sigma$), the system enters into the so-called *Mollow* regime[21], which is characterized by its emission spectrum in the shape of a triplet, with a central line flanked by a pair of symmetric peaks. An archetypal spectrum of a driven 2LS with $\Delta = 0$ is shown as a

dashed line in Fig. 1a. The origin of the three peaks has a natural explanation in the context of the "dressed atom" picture[58]: the energy structure of the 2LS becomes "*dressed*" by the laser, thus creating a ladder of energy manifolds, each of them composed of two energy levels, which we note as $|+\rangle$ and $|-\rangle$. Such a picture allows us to relate each of the four possible transitions between consecutive energy manifolds [shown in the inset of panel (a), where the transitions are indicated with colored arrows] to the emission peaks. Namely, the transition $|+\rangle \to |-\rangle$ (shown in blue) gives rise to the high-energy peak at frequency ω_+, the transition $|-\rangle \to |+\rangle$ (shown in red) originates the low-energy peak at frequency ω_-, and the degenerate transitions $|\pm\rangle \to |\pm\rangle$ (shown in green) correspond to the central peak at the frequency of the laser. The intensity of these peaks, as well as the energies $\omega_\pm$, vary when the driving laser is taken out of resonance from the 2LS. Namely, the triplet splits further and the satellite peaks become the dominant feature of the spectrum, as the central line loses its intensity. This is shown in solid lines in Fig. 1a. In general, the transitions that yield the spectrum are obtained through the diagonalization of the Liouvillian of the system[55]. Namely, rewriting the master Eq. (2) as $\partial_t\rho = -M\rho$, one can find the energy of the transitions as the imaginary part of the eigenvalues of the matrix M (their real parts correspond to the linewidth of the transition, which we show in the Methods section). Figure 1c shows in solid lines the three energy lines available for the emission of the 2LS driven out of resonance. For comparison, we also show in dashed lines the energies that unfold when the excitation is resonant [and which give rise to the spectrum shown in dashed lines in panel (a)]. The main distinction between these two cases is that in the detuned case the lines are always splitted, even in the limit when $\Omega/\gamma_\sigma \to 0$. In the opposite regime, when the intensity of the excitation dominates over the detuning, i.e., when $\Omega \gg \Delta$, the splitted lines coincide again. For intermediate intensities, the energy lines are approximately given by $\omega_\pm = \omega_L \pm \sqrt{4\Omega^2 + \Delta^2}$ (the exact expression that takes into account the dissipation is given in ref. [16]). Finally, note that the transitions with energies $\omega_\pm$ are associated to quantum jumps that change the quantum state of the 2LS, and therefore the same transition cannot take place twice in a row. In fact, in the next section, we will show that such a behavior can be exploited as a scheme for photon heralding in the regime with $\Delta \gtrsim \Omega$, where the transitions $|\pm\rangle \to |\mp\rangle$ become the dominant emission process.

Measurement of the photons

A key aspect of quantum mechanics is that measurements affect the quantum state of the system under observation. Thus, a correct description of the emission from the 2LS should also incorporate into the dynamics the effect of the observation by a physical detector. Such a description can be done with the theory of frequency-resolved correlations[13], implemented through the formalism of *cascaded systems*[59,60]. Thus, the detection of photons emitted from the 2LS at frequencies ω_1 and ω_2 by detectors of linewidth Γ_1 and Γ_2 can be described through the upgraded master equation (cf. Section I of the supplementary material for the derivation of the master equation for a single detector, and the generalization to N detectors)

$$\begin{aligned}
\partial_t\rho = {} & i[\rho, H_\sigma + H_d] + \frac{\gamma_\sigma}{2}\mathcal{L}_\sigma(\rho) + \frac{\Gamma_1}{2}\mathcal{L}_{a_1}(\rho) + \frac{\Gamma_2}{2}\mathcal{L}_{a_2}(\rho) \\
& - \sqrt{\gamma_\sigma\Gamma_1/2}\left\{[a_1^\dagger, \sigma\rho] + [\rho\sigma^\dagger, a_1]\right\} \\
& - \sqrt{\gamma_\sigma\Gamma_2/2}\left\{[a_2^\dagger, \sigma\rho] + [\rho\sigma^\dagger, a_2]\right\},
\end{aligned} \qquad (3)$$

where H_σ is the Hamiltonian in Eq. (1), $H_d = (\omega_1 - \omega_L)a_1^\dagger a_1 + (\omega_2 - \omega_L)a_2^\dagger a_2$ is the Hamiltonian describing the internal degrees of freedom of the detectors (namely, their free energy), and $a_k^\dagger$ and a_k are the bosonic creation and annihilation operators associated to the kth detector.

Using the master Eq. (3), we gain access to the frequency-resolved correlations of the emission from the Mollow triplet. In particular, we are interested in the second-order correlation between photons emitted at the frequencies of the satellite peaks (with energies $\omega_\pm$, c.f. the scheme in Fig. 1)
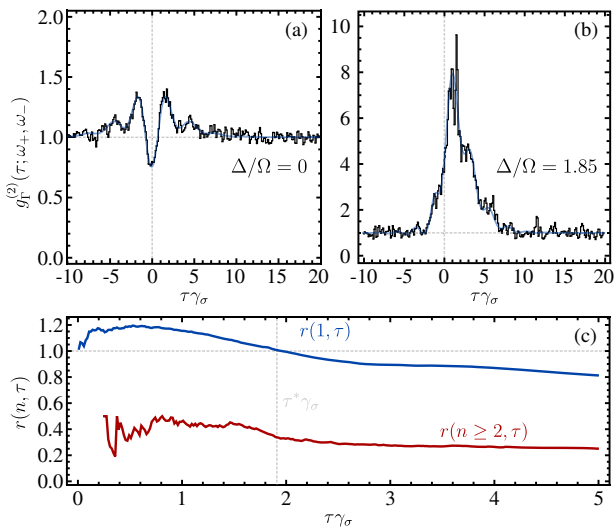
Fig. 2 | Heralded single photons observed through a frequency-resolved quantum Monte Carlo simulation. a, b Crossed-correlations between photons detected with frequencies ω_+ and ω_-, showing the agreement with theoretical prediction (solid blue lines) and the quantum Monte Carlo simulation (black bars). When the driving laser is resonant to the 2LS, the correlation function is completely symmetric (cf. panel **a**). When the driving is taken out of resonance, the shape of the correlation function resembles a λ, indicating that the emission of a photon with frequency ω_+ heralds the emission of a photon with frequency ω_- (cf. panel **b**). **c** Ratios $r(n, \tau)$ $= p(n, \tau, \Delta)/p(n, \tau, 0)$ of the probability to detect one (blue) and two or more (red) photons after detecting the heralding photon, when the driving is made out of resonance and in resonance. Taking the laser out of resonance enhances the single-photon heralding probability within a time-window τ^* of almost two lifetimes of the 2LS, as indicated by the dashed vertical line. Additionally, the probability to herald two or more photons is suppressed when the driving is done out of resonance. For the figures, we used γ_σ as the unit, $\Omega/\gamma_\sigma = 1$, $\Gamma/\gamma_\sigma = 1$, and the optimal detuning that, as we shall show in the next section, optimizes the entangled emission, namely $\Delta = 1.85\Omega$.

separated by a time τ, i.e., we compute

$$g_\Gamma^{(2)}(\tau, \omega_1, \omega_2) = \frac{\langle a_1^\dagger a_2^\dagger(\tau) a_2(\tau) a_1 \rangle}{\langle a_1^\dagger a_1 \rangle \langle a_2^\dagger a_2 \rangle}, \qquad (4)$$

for the case where $\omega_1 = \omega_+$ and $\omega_2 = \omega_-$. When the 2LS is driven resonantly, its $g_\Gamma^{(2)}(\tau, \omega_+, \omega_-)$ is completely symmetric, as shown in Fig. 2a. Such a shape indicates that there is no causal relation in the emission from the sidebands, and the photons are emitted without a preferential order. Note, however, that the inclusion of detection into the description of the emission leads to a loss of antibunching of the signal[61], as gaining knowledge about the frequency at which the photons are emitted spoils their perfect temporal resolution. The symmetric shape of the correlation is broken when the driving laser is taken out of resonance from the 2LS. Figure 2b shows the case for $\Delta = 1.85\Omega$, where it is clear that the emission from the high-energy sideband occurs *after* the emission of a photon from the low-energy one (the reverse situation occurs if the detuning becomes negative). While the type of correlation shown in Fig. 2b is indicative of a heralded emission, it does not necessarily imply that the emission consists of single photons. To show that this is in fact the case, we performed a frequency-resolved quantum Monte Carlo simulation[62] of the emission from the two sidebands of the Mollow triplet to compare the cases when the 2LS is driven in and out of resonance. Thus, from the simulations, we are able to obtain the probability $p(n, \tau, \Delta)$ to detect n photons of energy ω_+ within a time-window τ after a photon of energy ω_- has been measured, provided that the detuning between the 2LS and the laser is Δ. Figure 2c shows the ratios $r(n, \tau) = p(n, \tau, \Delta)/p(n, \tau, 0)$, which illustrate that the detuning enhances the probability to detect one photon by about 20% (blue line) while simultaneously decreases the probability to detect two or more photons (red

line). Note that the ratio $r(1, \tau)$ becomes less than one for time windows larger than $\tau^* \approx 2/\gamma_\sigma$, shown as a vertical dashed line in Fig. 2c. Thus, the heralded photons are more likely to be emitted within the time window $\tau \leq \tau^*$ when the 2LS is driven out of resonance. Together, Fig. 2b, c are the evidence that demonstrates that a 2LS driven out of resonance by a laser is a source of heralded single photons, whose frequencies correspond to the energies of the sidebands of the Mollow triplet.

Source of entangled photon pairs

Now that we have established that the emission from the satellite peaks of the detuned Mollow triplet is composed of highly correlated pairs of single photons, and that their emission can be observed in a heralded fashion, we investigate another type of quantum correlation: entanglement. It has been theoretically predicted[17] and experimentally observed[15] that pairs of photons emitted from the Mollow spectrum at various frequencies violate the Cauchy–Schwarz inequality (CSI), which can only happen in systems displaying entanglement[63]. Thus, in our article, we quantify entanglement through the so-called *logarithmic negativity* $\mathcal{N}(\rho)$[64–66], which is an entanglement monotone[67] that quantifies the degree to which the partial transposition of the quantum state violates the criterion of positivity[68].

Previous investigations on the Mollow triplet have shown that one can always find pair of frequencies $\tilde{\omega}_1$ and $\tilde{\omega}_2$ for which the CSI is violated[17], even when the laser is resonant to the 2LS. However, although such a violation is an indication of entanglement, the logarithmic negativity only becomes nonzero when the laser is taken out of resonance from the 2LS. Figure 3a shows the maximum $\mathcal{N}(\rho)$ that can be extracted from photons emitted at the sidebands, depending on both the intensity of the driving Ω and the linewidth of the detector Γ. Here, each point is obtained for the optimum detuning Δ_{opt} between the laser and the 2LS, which we display in Fig. 3b. While for most of the figure, the detuning that optimizes the entanglement is around $\Delta \sim 2\Omega$, in the upper left corner of the panel we find a region for which the optimal condition is found near resonance. However, looking at the map of the CSI violation, shown in Fig. 3c, we find that such a region is compatible with a classical state, as the ratio R (cf. Eq. (10) in the Methods section) falls below one. For visual aid, we have added the $R = 1$ contour as a red dashed line in all the panels. The behavior of the CSI, together with the artificial disruption in the logarithmic negativity, can be understood as a consequence of the competition of the detectors for photons emitted from the two sidebands. We parameterized such a contest through the ratio between the spectral window of detection Γ and the detuning between the entangled photons and the laser $\Delta_+ = (\omega_+ - \omega_L)$, as shown in Fig. 3d: the CSI violation starts precisely when this ratio becomes strictly less than one, and the photons emitted from the lateral peaks become distinguishable in frequency. Finally, in Fig. 3e, we show the emission rate of our source, i.e., $I = \Gamma\langle a^\dagger a \rangle$, as a function of the intensity of the laser and the linewidth of the detectors [the detuning between the 2LS and the laser is taken as in panel (b)], thus making evident the interplay between the quantity and the quality of the signal: the highest degree of entanglement is found when the peaks are very well separated from each other (i.e, $\Omega/\gamma_\sigma \gg 1$) and the linewidth of the observer is narrow (with Γ/γ_σ as small as possible), which in turn comes with the price that such a narrow linewidth decreases the emission rate of the source. In fact, in the configurations realized in the bottom right corner of the panels of Fig. 3, the quantum state of the pairs of entangled single photons is described—with 97% fidelity—as the superposition of the vacuum and the state $\tilde{\rho} \equiv |\Phi^-\rangle\langle\Phi^-|$ (cf. the Methods section). The latter is given by the Bell state

$$|\Phi^-\rangle = \frac{1}{\sqrt{2}}(|0, 0\rangle - |1, 1\rangle), \qquad (5)$$

with a purity of 91.6%, and a contribution to the full quantum state of 0.6%. Such a small percentage indicates that, although the photons are maximally entangled, one needs to wait for them to be emitted. Furthermore, we find that entanglement is spoiled as the linewidth of the detectors becomes large as compared to the emission lines of the triplet. This is because wide detectors
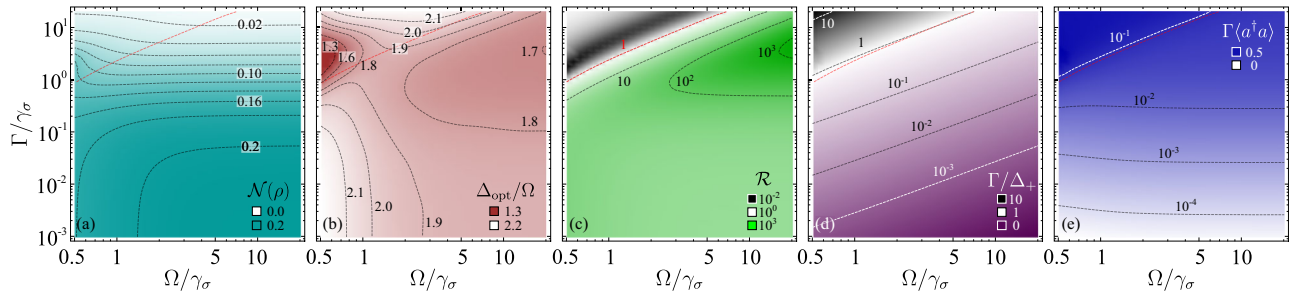
Fig. 3 | Characterization of our source of entangled pairs of single photons.
a Maximum logarithmic negativity that can be reached as a function of the linewidth of the detectors and the intensity of the driving laser, which indicates that the optimal condition for extracting entanglement is to have narrow detectors observing a Mollow triplet with a very large splitting (namely, the bottom right corner of the panel). **b** The optimum detuning at which the 2LS must be driven depends both on the intensity of the driving and the linewidth of the detectors or, equivalently, the optical targets receiving the entangled photons. **c** Violation of the CSI showing the regions where the negativity obtained in (**a**) is not an artifact of the competition between the detectors for the photons of the sidebands. **d** The ratio between the linewidth of the detectors and the splitting between the sidebands. It shows that the best configurations are those for which this ratio is as small as possible, and that it has to be less than 1 to violate the CSI. **e** Emission rate from the detectors, thus completing the mapping of the quality and the brightness of the source of entangled single photons based on the Mollow triplet. The red, diagonal, dotted line on each panel indicates the boundary above which the emission does not violate the CSI.

effectively erase the spectral information of the photons, and the emission from the sidebands becomes indistinguishable. However, one can overcome such an issue by driving the 2LS deeper into the Mollow regime, i.e., increasing the intensity of the laser, and thus taking the satellite peaks further away from each other. Notably, the pair of parameters (Ω, Δ) that optimize the logarithmic negativity between the photons from the sidebands of the triplet do not optimize the violation of the CSI nor maximize their second-order correlation function (cf. Section II of the Supplemental Material).

Entangling polaritons

A direct application of the results presented in the previous section is the excitation of one of the most ubiquitous systems in condensed matter physics; namely a pair of coupled bosonic fields. While the latter can represent a large variety of quantum systems, in the following, we will associate them to the so-called exciton-polaritons (henceforth, simply *polaritons*); which are pseudo-particles arising from the strong coupling between a photon and an exciton, either within a semiconductor microcavity[57] or on an organic sample[69,70]. The Hamiltonian describing polaritons can be written as

$$H_p = (\omega_a - \omega_L)a^\dagger a + (\omega_b - \omega_L)b^\dagger b + g(a^\dagger b + b^\dagger a), \quad (6)$$

where the photons and excitons have frequencies ω_a and ω_b, respectively; and they are coupled with strength g. Here, $a^\dagger$ (a) and $b^\dagger$ (b) are, correspondingly, the creation (annihilation) operators associated to the photonic and excitonic fields. Thus, the dynamics of polaritons driven by resonance fluorescence is given by the master Eq. (3), replacing H_d with the polariton Hamiltonian in Eq. (6), letting $a_1 \to a$, $a_2 \to b$, and introducing $\Gamma_1 = \Gamma_a$ and $\Gamma_2 = \Gamma_b$, as the decay rates of the photon and exciton modes of the polaritons. For the following discussion, we assume that the polaritons are in the strong coupling regime, in which the energy states become dressed and the light emitted is observed at the frequencies of the lower- and upper-polariton branches (cf. the full derivation in the *Methods* section). Figure 4a shows the concurrence between the polariton branches *after* the vacuum contribution has been removed through a post-selection process. We find that for entanglement to be observed, it is necessary that: (i) the polariton light-matter coupling should be larger than the decay of our source (we find that $g/\gamma_\sigma \approx 50$ is typically enough) and (ii) the photonic decay rate has to be of the order of magnitude or larger than the rate at which the source is emitting light, namely $\Gamma_a/\gamma_\sigma \geq 1$. The first condition prevents the excitations to the localized in a single polariton branch, while the latter guarantees that there are at most two polaritons in the system, thus maintaining strong correlations between the particles. The polariton quantum state that yields the maximum concurrence is shown in Fig. 4b before and in Fig. 4c after a post-selection process removing the vacuum contribution (see the Methods section for the details).
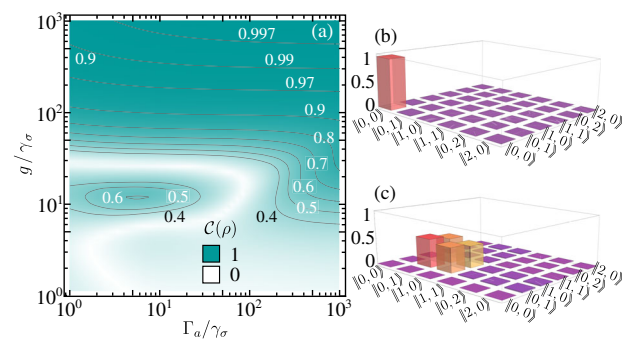

Fig. 4 | Maximally entangled polaritons. a Concurrence between the lower- and the upper-polariton branches, reaching up to 91% (cf. the *Methods* section for the details). **b** Quantum state tomography of the quantum state of polaritons. **c** Same as (**b**) after a post-selection process removing the vacuum. The remaining quantum state has a 0.997 fidelity with a superposition of vacuum and the Bell state $||\Psi^-\rangle\rangle$. The figure has been done using the parameters that optimize the entanglement of the photons emitted by the source, namely $\Omega/\gamma_\sigma = 4.9$, $\Delta/\gamma_\sigma = 8.92$ and letting the photon and the exciton be in resonance with the higher- and lower-energy sideband of the triplet, respectively. For (**b**) and (**c**), we have also used the parameters that yield the maximum concurrence between the polaritons, i.e., $\Gamma_a/\gamma_\sigma = 10$, $g/\gamma_\sigma \approx 300$ and $\Gamma_b \ll \Gamma_a$.

Here, we find that the quantum state of the polaritons has a 0.997 fidelity with a superposition between vacuum and the Bell state $||\Psi^-\rangle\rangle = \frac{1}{\sqrt{2}}(||0, 1\rangle\rangle - ||1, 0\rangle\rangle)$, where we have used the notation $||m, n\rangle\rangle$ to label a Fock state of polaritons (cf. the Methods section). These remarkable results show the power of our source of entangled photons, while providing further evidence supporting the observation that polaritons sustain entanglement[56], which makes them an attractive platform to perform, e.g., quantum communication and cryptography. These applications, however, lay outside the scope of this article and will be left for future research.

Discussion

We have described a novel source of entangled photon pairs, based on the Mollow triplet regime of Resonance Fluorescence. In fact, we showed that when the laser driving the two-level system (2LS) becomes detuned from the natural frequency of the 2LS, the lateral peaks of the triplet become the dominant feature of the emission spectrum. Thus, using the theory of frequency resolved correlations[13] we showed that, when one focuses on the photons emitted from such lateral peaks, one finds that their emission is heralded. Considering the dressed-atom picture, we showed that these photons, emitted at frequencies ω_+ and ω_- (cf. the scheme in Fig. 1), are the result of two atomic transitions that change the quantum state of the 2LS, and

therefore cannot take place twice in a row. Instead, they alternate in such a way that the emission of a photon ω_+ favors the emission of a photon ω_- (note that the opposite order can be achieved if the laser is blue- instead of red-shifted with respect to the 2LS). We have used a quantum Monte Carlo simulation to show that, taking the laser out of resonance from the 2LS, not only leads to the heralding behavior, but also suppresses emissions consisting of more than one photons; namely, our system operates as a source of heralded single photons.

Analysing the quantum correlations between the single photons emitted from the lateral peaks of the detuned Mollow triplet, we find that they are emitted in a superposition of vacuum and the Bell state $|\Phi^-\rangle$. Furthermore, we have delimited the region in the parameter space for which the photons violate the Cauchy–Schwarz inequality. Thus, we find that for the photons to display quantum energy-time entanglement, the linewidth of the detector—or, more generally, the optical target of the emission—has to be narrower than the separation between the lateral peaks of the triplet. Otherwise, the degree of indistinguishability of the photons emitted from the two peaks decreases, which in turn leads to the loss of entanglement. Furthermore, we showed the relation between the emission rate of our source and the degree of entanglement, as measured through the logarithmic negativity. In the *Methods* section, we have provided a table with the emission rate that our source would have if implemented with already-made experiments showing the appearance of the Mollow triplet. In all the cited cases, our source is able to provide, at least, tens of thousands of entangled photon pairs per second. Thus, our manuscript can be used as a road map for the experimental implementation of a source of entangled photons based on Resonance Fluorescence.

Lastly, to demonstrate the power of our source, we used it to excite an ubiquitous quantum system, commonly recurring in condensed-matter physics, namely a pair of coupled harmonic oscillators embedded in a dissipative environment. Thus, we use the example of exciton-polaritons (although our results are also applicable to systems composed or containing phonons, plasmons, bosonic nanoparticles, and photonics in general) and showed that our source is capable to inject entangled particles into the polariton system, and that, in turn, they are able to maintain such quantum correlations in spite of the decoherence introduced by spontaneous decay. We note that our model for polaritons has already been used to explain experimental results[56], and while further elements of decoherence may be relevant in the analysis of the entanglement in polaritons, their consideration would take us far away from the scope of the present paper and, therefore, they are left for future references.

Methods
Quantum optical formulation of the Cauchy–Schwarz inequality
The Cauchy–Schwarz inequality (CSI) is a fundamental result of mathematical analysis, which states that the inner product between two vectors, $\vec{u}$ and $\vec{v}$, cannot be larger than the product between the norms of each of the vectors, namely

$$|\langle \vec{u} \mid \vec{v}\rangle|^2 \leq \langle \vec{u} \mid \vec{u}\rangle \cdot \langle \vec{v} \mid \vec{v}\rangle, \tag{7}$$

where $\langle \cdot \mid \cdot \rangle$ indicates inner product. In the context of optics, the CSI applies to the intensities and correlations between fields, and Eq. (7) becomes

$$|\langle I_1 I_2\rangle|^2 \leq \langle I_1^2\rangle\langle I_2^2\rangle, \tag{8}$$

where I_1 and I_2 are the intensities of (fluctuating) fields, and $\langle \cdot \rangle$ indicates mean value. While classical states satisfy Eq. (8), in quantum mechanics one can encounter states whose correlations are larger than those allowed by the CSI[71,72]. Therefore, the violation of the CSI is used as an indicator of non-classicality. In fact, the violation of the CSI has been recently linked with the appearance of entanglement[73,74].

In this Article, we deal with the entanglement between photons emitted from the lateral peaks of the Mollow triplet, namely with frequencies $\omega_\pm$. The observables of these photons are unveiled by letting them excite a pair of

detectors, which have a finite linewidth, have natural frequencies that match the energy of the sidebands, and are described with annihilation operators a and b, both following Bose algebra. Thus, using the formalism of the second quantization, the inequality in Eq. (8) can be formulated in terms of the equal-time second-order correlation function of the operators of the detectors, namely

$$\left[G_{a,b}^{(2)}\right]^2 \leq G_{a,a}^{(2)} G_{b,b}^{(2)}, \tag{9}$$

where $G_{c,d}^{(2)} = \langle c^\dagger d^\dagger dc\rangle$ for $c, d \in \{a, b\}$. Thus, to quantify the degree of violation of the CSI, we introduce the coefficient

$$R = \frac{\left[G_{a,b}^{(2)}\right]^2}{G_{a,a}^{(2)} G_{b,b}^{(2)}}, \tag{10}$$

which is larger than one when the CSI is violated, i.e., when the state of the detectors is non-classical.

Linewidth of the entangled photons
In the main text, we indicated how to obtain the energy and linewidths of the energy transitions that arise from the Hamiltonian of our system. The strategy consists of writing the Master equation, e.g., given in Eq. (2), in a matrix way as $\partial_t \rho = -M\rho$, where ρ is the vector representation of the density matrix our system, and M is the matrix representation of the Liuvillian, e.g., the left-hand side of Eq. (2). The matrix M can be understood as a generalization to lossy systems of the Hamiltonian. As such, the (complex-valued) eigenvalues of M, which can be written as $\omega_j + i\gamma_j$, correspond to the energy (real part) and linewidth (imaginary part) of the emission lines of the system. Thus, in Fig. 5, we show the dependency of the linewidth of the peaks of the Mollow triplet, as a function of the intensity of the driving, Ω, and the detuning between the driving laser and the 2LS, Δ. There, we show the linewidths of the lateral peaks (solid blue) and the central line (dashed red) as a function of the detuning Δ, for the case in which the peaks of the triplet are well defined, namely, when $\Omega > \gamma_\sigma$. Note that the linewidth of the sidebands start with $\gamma_L = 3\gamma_\sigma/2$ at resonance, and transitions to $\gamma_L = \gamma_\sigma$ in the limit of large detuning, showing that the latter matches the almost bare emission of the 2LS. In the regime at which our source operates, namely with $\Delta \approx 2\Omega$ (note the vertical grid line), the linewidth of the lateral peaks is $\gamma_L \approx 5\gamma_\sigma/4$. Interestingly, the *observed* linewidth of the photons is modified by the detectors. In the limit where $\Gamma \to \infty$, the detector cannot distinguish the frequencies of the emitted photons, and as a consequence one would observe the "theoretical" emission spectrum, with the lateral peaks retaining their γ_L linewidth. In this scenario, the emission behaves as if it were not observed at all. In the opposite regime (which is where our source works the best), where the linewidth of the detector is very small, namely $\Gamma \ll \gamma_\sigma$, the emitted photons would have the linewidth inherited from the detector, i.e., Γ. Of course, the latter can be tuned using detectors with different linewidths or, equivalently, using filters before the detectors.

Bell state contribution
The steady-state solution of the master Eq. (3) provides us with the full density matrix, $\tilde{\rho}_{ss}^{full}$, of our source, as observed by two detectors. Thus, the quantum state of the light emitted from our source is obtained by tracing out the degrees of freedom of the 2LS, namely, we define

$$\rho_{ss}^{source} \equiv \mathrm{Tr}_\sigma\{\tilde{\rho}_{ss}^{full}\}, \tag{11}$$

where $\mathrm{Tr}_\sigma\{\cdot\}$ indicates the partial trace over the Hilbert space of the 2LS.

In the configurations realized in the bottom right corner of the panels of Fig. 3, the quantum state of our source can be approximated as

$$\rho_{ss}^{source} \approx (1 - \alpha)|0, 0\rangle\langle 0, 0| + \alpha\tilde{\rho}, \tag{12}$$
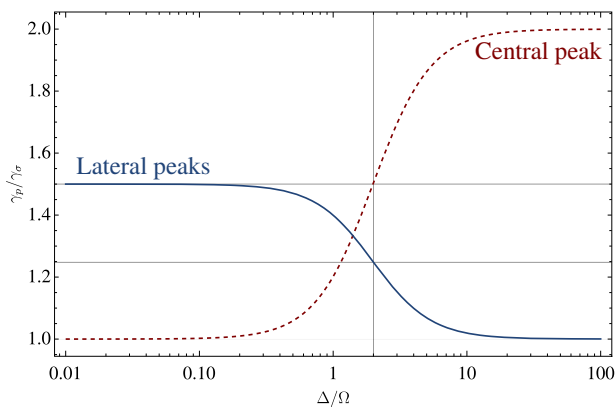
Fig. 5 | Linewidth of the lateral and central peaks of the Mollow triplet (which is obtained for $\Omega > \gamma_\sigma$), as a function of the detuning between the driving laser and the 2LS. In the regime at which our source operates, namely with $\Delta \approx 2\Omega$ (note the vertical grid line), the linewidth of the lateral peaks is $\gamma_L \approx 5\gamma_\sigma/4$.

which reaches a fidelity of 97% with a mixture between the vacuum and the Bell state $|\Phi^-\rangle$, namely

$$\rho_{th} = (1 - \alpha)|0,0\rangle\langle 0,0| + \alpha|\Phi^-\rangle\langle\Phi^-|, \quad (13)$$

with $\alpha = 0.6\%$. Finally, keeping α fixed, we are able to determine that $\tilde{\rho}$ in Eq. (12) has a purity of 91.6%.

Concurrence from polaritons
The polariton Hamiltonian (6) describes the coherent interaction between a photon and an exciton. In the strong coupling regime, the energy levels of Hamiltonian hybridize, and the luminescence of the system takes place at the frequencies of the so-called *dressed states* of the system (mathematically, they are the states that diagonalise the Hamiltonian). Commonly, such states are referred to as the upper- and lower-polariton branches, and they are formally described with annihilation operators u and l, respectively. The latter two are related to the operators of the photon and of the exciton in the following way

$$l = \chi_+ a - \chi_- b, \quad (14a)$$

$$u = \chi_- a + \chi_+ b, \quad (14b)$$

where we have introduced the so-called Hopfield coefficients

$$\chi_\pm = \frac{1}{\sqrt{2}}\left(1 \pm \frac{\delta}{\sqrt{\delta^2 + 4g^2}}\right)^{1/2}, \quad (15)$$

and we have used the notation notation $\delta = \omega_b - \omega_a$. Using the transformation in Eq. (14) the Hamiltonian in Eq. (6) becomes $H_P = (\omega_l - \omega_L) l^\dagger l + (\omega_u - \omega_L)u^\dagger u$, with the energies of the polariton branches defined as

$$\omega_l = \frac{1}{2}\left(\omega_a + \omega_b - \sqrt{\delta^2 + 4g^2}\right) \quad (16a)$$

$$\omega_u = \frac{1}{2}\left(\omega_a + \omega_b + \sqrt{\delta^2 + 4g^2}\right). \quad (16b)$$

Naturally, using the operators defined in Eq. (14), one can define Fock states of polaritons as

$$\|m,n\rangle = \frac{1}{\sqrt{m!n!}} l^{\dagger m} u^{\dagger n}\|0,0\rangle, \quad (17)$$

namely, a state with m and n particles in the lower and upper branch, respectively.

Although polaritons are described as a bosonic field, when we excite them with the source of entangled photons described in the main text, we can safely assume that there are, at most, two excitations within the system. This means that one can limit the Hilbert space of the system and study the polariton entanglement by turning to a so-called *detection matrix* $\bar{\theta}$[56]. The latter is constructed from mean values of the density matrix ρ_{ss} obtained as a steady-state solution to the master Eq. (5) of the main text, namely

$$\bar{\theta} \equiv \frac{1}{\mathcal{N}}\begin{pmatrix} \langle\langle 0,0\|\rho_{ss}\|0,0\rangle\rangle & \langle\langle 0,0\|\rho_{ss}\|1,0\rangle\rangle & \langle\langle 0,0\|\rho_{ss}\|0,1\rangle\rangle & \langle\langle 0,0\|\rho_{ss}\|1,1\rangle\rangle \\ h.c. & \langle\langle 1,0\|\rho_{ss}\|1,0\rangle\rangle & \langle\langle 1,0\|\rho_{ss}\|0,1\rangle\rangle & \langle\langle 1,0\|\rho_{ss}\|1,1\rangle\rangle \\ h.c. & h.c. & \langle\langle 0,1\|\rho_{ss}\|0,1\rangle\rangle & \langle\langle 0,1\|\rho_{ss}\|1,1\rangle\rangle \\ h.c. & h.c. & h.c. & \langle\langle 1,1\|\rho_{ss}\|1,1\rangle\rangle \end{pmatrix}. \quad (18)$$

In the definition of the detection matrix, we have included the normalization constant $\mathcal{N}$ which guarantees that $\text{Tr}(\bar{\theta}) = 1$, and $h.c.$ indicates the hermitian conjugate of the matrix element. Then, from the matrix in Eq. (18), we obtain the concurrence as $\mathcal{C}(\bar{\theta}) \equiv \max(0, \lambda_1 - \lambda_2 - \lambda_3 - \lambda_4)$ where the λ_i are the eigenvalues in decreasing order of the matrix $\sqrt{\sqrt{\theta}\tilde{\theta}\sqrt{\theta}}$, where $\tilde{\theta} \equiv (\sigma_y \otimes \sigma_y)\bar{\theta}^T(\sigma_y \otimes \sigma_y)$, and σ_y is a Pauli spin matrix. Finally, the post-selection consists in dropping from the matrix in Eq. (18) the terms involving the vacuum polariton states (i.e., the first row and the first column) and renormalizing the resulting matrix.

Experimental parameters for implementation
Our source of entangled photons relies on the coherent excitation of a two-level system. The latter can be implemented in a variety of platforms, thus endowing our source with the ability to tune the energies of the entangled photons. In Table 1, we show the parameters extracted from experiments where the Mollow triplet has been successfully observed. Although the decay rates are overall comparable across the various platforms, with differences of

Table 1 | Relevant parameters extracted from experimental realizations of the Mollow triplet in various platforms, including semiconductor quantum dots (S.Q.D.), molecules, cold atoms and artificial atoms (A.A.) implemented in superconducting circuits

Platform	λ_0	$\gamma/2\pi$ (MHz)	$\Delta\lambda$	I (photons/s)	Ref.
S.Q.D.	925 nm	180	0.05 nm	5.65×10^5	[22]
	914 nm	1000	0.31 nm	31.41×10^5	[23]
	915 nm	337	0.11 nm	10.59×10^5	[24]
	780 nm	343	0.08 nm	10.78×10^5	[25]
	914 nm	287	0.09 nm	9.02×10^5	[26]
	914 nm	1000	0.31 nm	31.41×10^5	[27]
Molecule	590 nm	17–20	2 pm	6.28×10^4	[28]
Cold atoms	780 nm	6.07	1 pm	1.91×10^4	[29,30]
A.A.	29.4 mm	57	20.6 mm	1.79×10^5	[32]
	46.9 mm	26	3.48 mm	8.17×10^4	[33]
	62.5 mm	13	19.6 mm	4.08×10^4	[33]
	41.1 mm	21	13.74 mm	6.59×10^4	[34]

Here we show λ_0, the resonance wavelength of the 2LS, the natural decay rate γ, the separation in wavelength $\Delta\lambda$ between the entangled photons (whose wavelengths are given by $\lambda_\pm = \lambda_0 \pm \Delta\lambda/2$), and the pair emission rate I, for which we have assumed the optimal detuning condition (i.e., $\Delta = 2\Omega$) and we have used $\Omega \approx 10\gamma$, which is a value easily accessible in all the experiments (in some of them Ω can even be considerably larger) of the table.

at most an order of magnitude, engineering artificial atoms to shift their resonant frequencies deeper into the infrared or even the microwave regions of the electromagnetic spectrum, allows to further split the wavelengths of the entangled photons. Finally, the emission rate has been obtained by assuming the parameters of Fig. 3 that provide a high degree of entanglement; namely, we have assumed $\Gamma/\gamma_\sigma = 10^{-1}$, $\Omega/\gamma_\sigma = 10$ and taken the corresponding value $\Gamma\langle a^\dagger a \rangle = 5 \times 10^{-3}$, which translate to tens to hundreds of thousand of entangled photon pairs per second.

Data availability
The data that supports the plots within this paper and other findings of this study are freely available at the Harvard Dataverse Repository as Supporting Data for "Entanglement in Resonance Fluorescence" (https://doi.org/10.7910/DVN/TLBG9X).

Code availability
The various codes used for modeling the data are available from the corresponding author upon reasonable request.

References
1. Kimble, H. J. & Mandel, L. Theory of resonance fluorescence. *Phys. Rev. A* **13**, 2123 (1976).
2. Allen, L. & Eberly, J. H. *Optical Resonance and Two-Level Atoms* (Dover, 1987).
3. Kimble, H. J., Dagenais, M. & Mandel, L. Photon antibunching in resonance fluorescence. *Phys. Rev. Lett.* **39**, 691 (1977).
4. Chang, D. E., Sørensen, A. S., Demler, E. A. & Lukin, M. A single-photon transistor using nanoscale optical transistor. *Nat. Phys.* **3**, 76 (2007).
5. Senellart, P., Solomon, G. & White, A. High-performance semiconductor quantum-dot single-photon sources. *Nat. Nanotech.* **12**, 1026 (2017).
6. Sinha, U. et al. Single-photon sources. *Opt. Photonics News* **30**, 32 (2019).
7. Fattal, D., Diamanti, E., Inoue, K. & Yamamoto, Y. Quantum teleportation with a quantum dot single photon source. *Phys. Rev. Lett.* **92**, 037904 (2004).
8. Beveratos, A. et al. Single photon quantum cryptography. *Phys. Rev. Lett.* **89**, 187901 (2002).
9. Dousse, A. et al. Ultrabright source of entangled photon pairs. *Nature* **466**, 217 (2010).
10. Gazzano, O. et al. Bright solid-state sources of indistinguishable single photons. *Nat. Comm.* **4**, 1425 (2012).
11. Loredo, J. C. et al. Scalable performance in solid-state single-photon sources. *Optica* **3**, 433 (2016).
12. Somaschi, N. et al. Near-optimal single-photon sources in the solid state. *Nat. Photon.* **10**, 340 (2016).
13. del Valle, E., González-Tudela, A., Laussy, F. P., Tejedor, C. & Hartmann, M. J. Theory of frequency-filtered and time-resolved N-photon correlations. *Phys. Rev. Lett.* **109**, 183601 (2012).
14. González-Tudela, A., Laussy, F. P., Tejedor, C., Hartmann, M. J. & del Valle, E. Two-photon spectra of quantum emitters. *New J. Phys.* **15**, 033036 (2013).
15. Peiris, M. et al. Two-color photon correlations of the light scattered by a quantum dot. *Phys. Rev. B* **91**, 195125 (2015).
16. López Carreño, J. C., del Valle, E. & Laussy, F. P. Photon correlations from the mollow triplet. *Laser Photon. Rev.* **11**, 1700090 (2017).
17. Sánchez Muñoz, C., del Valle, E., Tejedor, C. & Laussy, F. P. Violation of classical inequalities by photon frequency filtering. *Phys. Rev. A* **90**, 052111 (2014).
18. Díaz-Camacho, G. et al. Multiphoton Emission. https://doi.org/10.48550/ARXIV.2109.12049 (2021).
19. Zubizarreta Casalengua, E. Z., del Valle, E. & Laussy, F. P. Two-photon emission in detuned resonance fluorescence. *Phys. Scr* **98**, 055104 (2023).
20. Masters, L. et al. On the simultaneous scattering of two photons by a single two-level atom. Nature Photonics **17**, 972 (2023). https://doi.org/10.1038/s41566-023-01260-7
21. Mollow, B. R. Power spectrum of light scattered by two-level systems. *Phys. Rev.* **188**, 1969 (1969).
22. Konthasingheet, K. et al. Coherent versus incoherent light scattering from a quantum dot. *Phys. Rev. B* **85**, 235315 https://doi.org/10.1103/PhysRevB.85.235315 (2012).
23. Ulhaq, A. et al. Cascaded single-photon emission from the mollow triplet sidebands of a quantum dot. *Nat. Photon.* **6**, 238 (2012).
24. Muller, A. et al. Resonance fluorescence from a coherently driven semiconductor quantum dot in a cavity. *Phys. Rev. Lett.* **99**, 187402 (2007).
25. Vamivakas, A. N., Zhao, Y., Lu, C.-Y. & Atatüre, M. Spin-resolved quantum-dot resonance fluorescence. *Nat. Phys.* **5**, 198 (2009).
26. Flagg, E. B. et al. Resonantly driven coherent oscillations in a solid-state quantum emitter. *Nat. Phys.* **5**, 203 (2009).
27. Ates, S. et al. Post-selected indistinguishable photons from the resonance fluorescence of a single quantum dot in a microcavity. *Phys. Rev. Lett.* **103**, 167402 (2009).
28. Wrigge, G., Gerhardt, I., Hwang, J., Zumofen, G. & Sandoghdar, V. Efficient coupling of photons to a single molecule and the observation of its resonance fluorescence. *Nat. Phys.* **4**, 60 (2008).
29. Ortiz-Gutiérrez, L. et al. Mollow triplet in cold atoms. *New J. Phys.* **21**, 093019 (2019).
30. Ng, B. L., Chow, C. H. & Kurtsiefer, C. Observation of the Mollow triplet from an optically confined single atom. *Phys. Rev. A* **106**, 063719 (2022).
31. Cui, C., Zhang, L. & Fan, L. Photonic analog of Mollow triplet with on-chip photon-pair generation in dressed modes. *Opt. Lett.* **46**, 4753 (2021).
32. Astafiev, O. et al. Resonance fluorescence of a single artificial atom. *Science* **327**, 840 (2010).
33. van Loo, A. F. et al. Photon-mediated interactions between distant artificial atoms. *Science* **342**, 1494 (2013).
34. Toyli, D. M. et al. Resonance fluorescence from an artificial atom in squeezed vacuum. *Phys. Rev. X* **6**, 031004 (2016).
35. Bouchiat, V., Vion, D., Joyez, P., Esteve, D. & Devoret, M. H. Quantum coherence with a single copper pair. *Phys. Scr.* **1998**, 165 (1998).
36. Nakamura, Y., Pashkin, Y. A. & Tsai, J. S. Coherent control of macroscopic quantum states in a single-cooper-pair box. *Nature* **398**, 786 (1999).
37. Mooji, J. E. et al. Josephson persistent-current qubit. *Science* **285**, 1036 (1999).
38. Vion, D. et al. Manipulating the quantum state of an electrical circuit. *Science* **296**, 886 (2002).
39. Martinis, J. M., Nam, S., Aumentado, J. & Urbina, C. Rabi oscillations in a large Josephson-juction qubit. *Phys. Rev. Lett.* **89**, 117901 (2002).
40. Koch, J. et al. Charge-insensitive qubit design derived from the Cooper pair box. *Phys. Rev. A* **76**, 042319 (2007).
41. Schreier, J. A. et al. Suppressing charge noise decoherence in superconducting charge qubits. *Phys. Rev. B* **77**, 180502 (2008).
42. Bányai, L. & Koch, S. W. *Semiconductor Quantum Dots*. World Scientific Series on Atomic, Molecular, and Optical Physics No. vol. 2 (World Scientific, 1993).
43. O'Brien, J. L., Furusawa, A. & Vučković, J. Photonic quantum technologies. *Nat. Phys.* **3**, 687 (2009).
44. Lodahl, P., Mahmoodian, S. & Stobbe, S. Interfacing single photons and single quantum dots with photonic nanostructures. *Rev. Mod. Phys.* **87**, 347 (2015).

45. Grünwald, P. & Vogel, W. Entanglement in atomic resonance fluorescence. *Phys. Rev. Lett.* **104**, 233602 (2010).

46. del Valle, E. Distilling one, two and entangled pairs of photons from a quantum dot with cavity QED effects and spectral filtering. *New J. Phys.* **15**, 025019 (2013).

47. Akopian, N. et al. Entangled photon pairs from semiconductor quantum dots. *Phys. Rev. Lett.* **96**, 130501 (2006).

48. Stevenson, R. M. et al. A semiconductor source of triggered entangled photon pairs. *Nature* **439**, 179 (2006).

49. Schumacher, S. et al. Cavity-assisted emission of polarization-entangled photons from biexcitons in quantum dots with fine-structure splitting. *Opt. Express* **20**, 5335 (2012).

50. Johne, R. et al. Entangled photon pairs produced by a quantum dot strongly coupled to a microcavity. *Phys. Rev. Lett.* **100**, 240404 (2008).

51. Pathak, P. K. & Hughes, S. Generation of entangled photon pairs from a single quantum dot embedded in a planar photonic-crystal cavity. *Phys. Rev. B* **79**, 205416 (2009).

52. Sánchez Muñoz, C. et al. Emitters of N-photon bundles. *Nature Photon* **8**, 550 (2014).

53. López Carreño, J. C., Sánchez Muñoz, C., Sanvitto, D., del Valle, E. & Laussy, F. P. Exciting polaritons with quantum light. *Phys. Rev. Lett.* **115**, 196402 (2015).

54. López Carreño, J. C. & Laussy, F. P. Excitation with quantum light. I. Exciting a harmonic oscillator. *Phys. Rev. A* **94**, 063825 (2016).

55. López Carreño, J. C., Sánchez Muñoz, C., del Valle, E. & Laussy, F. P. Excitation with quantum light. II. Exciting a two-level system. *Phys. Rev. A* **94**, 063826 (2016).

56. Cuevas, Á. et al. First observation of the quantized exciton-polariton field and effect of interactions on a single polariton. *Sci. Adv.* **4**, eaao6814 (2018).

57. Weisbuch, C., Nishioka, M., Ishikawa, A. & Arakawa, Y. Observation of the coupled exciton-photon mode splitting in a semiconductor quantum microcavity. *Phys. Rev. Lett.* **69**, 3314 (1992).

58. Cohen-Tannoudji, C. N. & Reynaud, S. Dressed-atom description of resonance fluorescence and absorption spectra of a multi-level atom in an intense laser beam. *J. Phys. B. At. Mol. Phys.* **10**, 345 (1977).

59. Gardiner, C. W. Driving a quantum system with the output field from another driven quantum system. *Phys. Rev. Lett.* **70**, 2269 (1993).

60. Carmichael, H. J. Quantum trajectory theory for cascaded open systems. *Phys. Rev. Lett.* **70**, 2273 (1993).

61. López Carreño, J. C., Zubizarreta Casalengua, E., Silva, B., del Valle, E. & Laussy, F. P. Loss of antibunching. *Phys. Rev. A* **105**, 023724 (2022).

62. López Carreño, J. C., del Valle, E. & Laussy, F. P. Frequency-resolved Monte Carlo. *Sci. Rep.* **8**, 6975 (2018).

63. Gühne, O. & Tóth, G. Entanglement detection. *Phys. Rep.* **474**, 1 (2009).

64. Duan, L.-M., Giedke, G., Cirac, J. I. & Zoller, P. Inseparability criterion for continuous variable systems. *Phys. Rev. Lett.* **84**, 2722 (2000).

65. Simon, R. Peres-Horodecki separability criterion for continuous variable systems. *Phys. Rev. Lett.* **84**, 2726 (2000).

66. Vidal, G. & Werner, R. F. Computable measure of entanglement. *Phys. Rev. A* **65**, 032314 (2002).

67. Plenio, M. B. Logarithmic negativity: a full entanglement monotone that is not convex. *Phys. Rev. Lett.* **95**, 090503 (2005).

68. Horodecki, R., Horodecki, P., Horodecki, M. & Horodecki, K. Quantum entanglement. *Rev. Mod. Phys.* **81**, 865 (2009).

69. Plumhof, J. D., Stöferle, T., Mai, L., Scherf, U. & Mahrt, R. F. Room-temperature bose–einstein condensation of cavity exciton-polaritons in a polymer. *Nat. Mater.* **13**, 247 (2014).

70. Lerario, G. et al. Room-temperature superfluidity in a polariton condensate. *Nat. Phys.* **13**, 837 (2017).

71. Glauber, R. J. The quantum theory of optical coherence. *Phys. Rev.* **130**, 2529 (1963).

72. Reid, M. D. & Walls, D. F. Violations of classical inequalities in quantum optics. *Phys. Rev. A* **34**, 1260 (1986).

73. Kheruntsyan, K. V. et al. Violation of the Cauchy–Schwarz inequality with matter waves. *Phys. Rev. Lett.* **108**, 260401 (2012).

74. Wasak, T., Szańkowski, P., Ziń, P., Trippenbach, M. & Chwedeńczuk, J. Cauchy-Schwarz inequality and particle entanglement. *Phys. Rev. A* **90**, 033616 (2014).

Acknowledgements

Author contributions

J.C.L.C. proposed the idea. J.C.L.C. and S.B.F. developed the theoretical formalism and the conceptual tools, and then implemented the theoretical methods and analysed the data. J.C.L.C. and M.S. contributed material, analysis tools and expertize. J.C.L.C. wrote the main paper, the Supplemental Material, and supervised the research. All authors discussed the results and its implications and commented on the manuscript.

Competing interests

The authors declare no competing interests.

Additional information

Supplementary information The online version contains supplementary material available at https://doi.org/10.1038/s44310-023-00001-6.

Correspondence and requests for materials should be addressed to Juan Camilo López Carreño.

Reprints and permissions information is available at http://www.nature.com/reprints

Publisher's note Springer Nature remains neutral with regard to jurisdictional claims in published maps and institutional affiliations.